Intelligent Retrieval of Radar Reflectivity Factor With Privacy Protection Under Meteorological Satellite Remote Sensing

Huichao Lin, Xiaolong Xu, *Senior Member, IEEE*, Muhammad Bilal, *Senior Member, IEEE*, Yong Cheng, and Dongqing Liu

***Abstract*—Meteorological radar data are essential for meteorological monitoring, forecasting, and research, and it plays a crucial role in observing and warning of extreme weather risks. However, meteorological radars have some limitations, such as uneven distribution and severe topographical influence. Meteorological remote sensing satellites can partially overcome these limitations by providing larger observational scope and high spatial and temporal resolution. Using data from meteorological remote sensing satellites to train radar reflectivity factor retrieval models can effectively compensate for the missing and poor quality of radar data. However, there are still some challenges, such as extracting the features of intense convective weather with unclear coverage from complex multichannel meteorological remote sensing satellite data and removing the interference caused by nonprecipitation clouds on retrieval models. Moreover, the privacy and security of remote sensing data transmission need to be ensured. In this article, we propose a novel method that combines the advanced encryption standard method to protect the transmission of remote sensing data, a multiscale feature fusion module to extract multiscale features from multichannel meteorological remote sensing satellite data, and an attention technique to reduce the interference of nonprecipitation clouds on retrieval models. We conduct comparison experiments with multiple indicators to demonstrate that our method has certain advantages in retrieving radar reflectivity values of different sizes. Our method achieves 0.63, 0.36, 0.49, 0.55, and 0.99 on probability of detection, false alarm ratio, critical success index, Heidke skill score, and accuracy scores, respectively.**

***Index Terms*—Cryptography, deep learning, Hamawari-8, radar reflectivity factor (RF), remote sensing.**

Manuscript received 19 January 2023; revised 8 May 2023; accepted 7 July 2023. Date of publication 19 July 2023; date of current version 2 August 2023. This work was supported by Future Network Research Fund of Jiangsu Province under Grant FNSRFP-2021-YB-18. *(Corresponding author: Xiaolong Xu.)*

Huichao Lin and Yong Cheng are with the School of Software, Nanjing University of Information Science and Technology, Nanjing 210044, China (e-mail: 20211249431@nuist.edu.cn; yongcheng@nuist.edu.cn).

Xiaolong Xu is with the School of Software, Nanjing University of Information Science and Technology, Nanjing 210044, China, and also with the Jiangsu Collaborative Innovation Center of Atmospheric Environment and Equipment Technology (CICAEET), Nanjing University of Information Science and Technology, Nanjing 210044, China (e-mail: xlxu@ieee.org).

Muhammad Bilal is with the Department of Computer and Electronic Systems Engineering, Hankuk University of Foreign Studies, Yongin 17579, South Korea (e-mail: m.bilal@ieee.org).

Dongqing Liu is with Nanjing Meteorological Bureau, Nanjing 210044, China (e-mail: dqliu1986@sina.com).

Digital Object Identifier 10.1109/JSTARS.2023.3296908

I. Introduction

EXTREME weather catastrophes have been more frequent in recent years [1], with their suddenness, widespreadness, and destructive nature posing a grave threat to the safety of people's lives and property, attracting the attention of the whole population [2]. China is subject to a broad variety of natural disasters on account of its huge land, variable climate, and varied topography. Due to its concentrated and severe character, intense convective weather has long posed a challenging forecasting problem, with a short time frame and a tiny scale. Monitoring and recognizing the onset and evolution of intense convective weather with precision is essential for enhancing disaster defense capabilities and minimizing human and economic losses [3]. Consequently, reliable and high-quality meteorological measurements are crucial for weather forecasting and catastrophe warning.

With the ongoing development and enhancement of meteorological radar networks, high-resolution Doppler weather radar has become one of the most effective tools for evaluating and forecasting small-scale weather systems and monitoring and predicting extreme weather [4]. Currently, radar data have been developed and implemented in a variety of meteorological service applications [5]. There is a strong link between radar reflectivity factor (RF) and intensity of precipitation [6]. Precipitation may be mathematically calculated and projected using RF data.

In spite of this, there are still a few challenges that must be resolved in the application of RF. Meteorological radar is constrained by clutter interference, and radar signals are greatly reduced and accompanied by beam abnormalities in steep terrain locations. Moreover, the harsh geographical location environments and high maintenance costs of meteorological radar installations have resulted in a concentration of radar networks primarily in the central and eastern regions and along the coast of China, leaving significant radar coverage blind spots in the southwestern regions and limiting sea weather observation [7]. Satellite data offers substantial benefits over radar data in terms of coverage and temporal continuity, and may give exhaustive information on atmospheric conditions [8]. In recent years, satellite sensing technology has undergone fast development and several innovations, including an increase in the number of satellite sensing channels and vastly enhanced temporal and geographical resolutions [9]. Various meteorological aspects can

This work is licensed under a Creative Commons Attribution-NonCommercial-NoDerivatives 4.0 License. For more information, see https://creativecommons.org/licenses/by-nc-nd/4.0/

be recovered utilizing satellite-provided data, such as visible light, infrared radiation, atmospheric vertical detection, and microwave detection data.

In recent years, data-driven deep learning algorithms have garnered significant interest in the area of meteorology, with several academics investigating ways to leverage satellite data to gather RF data, enhance radar networks, and fill coverage blind spots. Recent technological advancements in deep learning have significantly accelerated this study process [10]. The method based on U-Net [11] was proposed to reconstruct multichannel satellite data features into RF data. Yang et al. [12] introduced attention mechanisms into the U-Net network to reduce the impact of interfering features during model training. However, these methods use repeated downsampling to extract features and repeated upsampling to restore resolution, which leads to a significant loss of spatial accuracy. In addition, due to the nonuniform coverage of severe weather and the interference of many nonprecipitating clouds in complex satellite multichannel data, such as convective clouds being often confused with precipitation clouds in temperature-sensitive infrared channels [13], it is difficult for retrieval models to extract key information from complex satellite data, resulting in a mediocre final retrieval effect. At the same time, meteorological satellite data usually include high-resolution cloud maps, meteorological data, and multichannel sensor parameters, which frequently contain national technological secrets. If unauthorized personnel obtain, use, or disclose this information, it will cause certain losses to relevant departments. Therefore, ensuring the transmission security of satellite data is crucial when receiving real-time satellite data for radar reflectivity retrieval.

To address the aforementioned issues, this article uses a fully convolutional neural network [14] to extract deep-level feature information from satellite multichannel data. Then, a multiscale feature fusion module is used to capture the characteristics of precipitation clouds with varying locations and sizes, and attention mechanism modules are introduced in each scale calculation module, including channel attention module and spatial attention module. The main purpose of the channel attention module is to enable the retrieval model to focus more on other channels that have not been interfered with when there is interference from nonprecipitation clouds in the channel information. The spatial attention module is designed to enable the model to focus more on the regional features of precipitation clouds. After parallel computation of these two modules, the current scale information features are obtained through weighted summation. Finally, multiple scale information features are concatenated and input into the decoding module to obtain the results.

The following are the principal contributions of this article.

1) The satellite data from the sender are encrypted using the advanced encryption standard (AES) algorithm and decrypted after ensuring receipt, in order to protect the data collected by the satellite from unauthorized access or tampering during transmission.
2) A multiscale feature fusion module (MFM) for RF retrieval model is proposed, which effectively acquires data characteristics of precipitation cloud clusters with varying sizes and positions using information features at different scales.
3) An attention mechanism module is introduced in MFM, wherein the spatial attention module enables the model to focus more on the areas where precipitation cloud clusters appear, while the channel attention module allows the model to focus more on the corresponding satellite channels.

II. Related Work

The core of predicting extreme weather events currently lies in solving the problem of accurate and reliable data sources and establishing the relationship between data and meteorological characteristics. Obtaining accurate, reliable, and complete data sources is the primary prerequisite for all other work. With the continuous development of satellite observation technology, significant progress has been made in satellite numerical retrieval research. However, it also faces many challenges, such as improving data quality, model accuracy, and computational efficiency, and increasing data volume. To overcome these challenges, researchers are constantly developing new methods and technologies, such as deep learning and Big Data analysis techniques.

Ba et al. [15] extracted the radiation properties and physical features of clouds, such as cloud top height, cloud optical thickness, and cloud phase, using multispectral satellite data to enhance precipitation retrieval techniques. Ebert et al. [16] discovered that strengthening the categorization of convective and stratiform precipitation improves the accuracy of satellite precipitation estimations; thus, several retrieval algorithms also prioritize the classification of convective-stratiform zones. Torricella et al. [17] discovered that cloud top height is reflective of convective precipitation intensity, and that the effective particle radius of ice clouds is proportional to precipitation intensity. Thies et al. [18] use Meteosat second-generation-spinning enhanced visible and infrared image data to identify convective/stratiform precipitation areas and precipitation intensity during the day and night by calculating precipitation probability matrices, employing brightness temperature and brightness temperature difference as cloud parameter information, including 8.7, 10.8, 12.1, and 10.8 μm. Feidas et al. [19] also utilize a similar SEVIRI satellite four multispectral infrared data combined threshold approach to categorize convective-stratiform precipitation. Lazri et al. [20] proposed the Mediterranean area scheme CS-RADT, which uses multichannel information to differentiate convective cloud regions and stratiform cloud regions, calibrated by instantaneous radar data to determine thresholds, and combined with rain gauge station data to calculate precipitation rates of different cloud regions.

China has a vast territory, and due to the influence of terrain, there are still significant blind spots in our country's meteorological radar network. Training a retrieval model of RF based on meteorological satellite data can partially compensate for the uneven distribution of meteorological radars and their susceptibility to terrain effects. Veillette et al. [21] used convolutional neural networks to construct synthetic radar images. The model

takes data from all visible and infrared channels of the GOES satellite, global lightning data, and numerical model data as input, generates seamless composite radar mosaics after training, and has higher accuracy and generalization ability than previous methods based on random forest. Duan et al. [11] used the U-Net network and five infrared channel data of the Himawari-8 satellite to study the radar combination reflectivity reconstruction task of convective storms in northern China. This method can effectively reproduce the location, shape, and intensity information of convective storms, but the U-Net network architecture is difficult to capture multiscale information from satellite data. Sun et al. [22] applied the U-Net network to Fengyun-4 satellite data, using infrared channel data and infrared temperature difference as model inputs, and effectively retrieval radar reflectivity. Yang et al. [12] introduced the attention mechanism into the U-Net-based retrieval model, effectively improving the accuracy of the retrieval model. However, the network architecture with repeated upsampling and downsampling also has the problem of losing spatial accuracy.

With the increasing use of satellite technology for data transmission, privacy concerns have become a major issue. To address this problem, researchers have proposed various methods to protect privacy during satellite data transmission. Jeon et al. [23] propose a cross-layer encryption technique that combines cyclic feedback mode (CFB), AES, and Turbo codes to improve the security and reliability of satellite data transmission. The work proposes a robust satellite image encryption scheme based on discretized chaotic maps and AES. Bensikaddour and Bentoutou [24] propose a robust satellite image encryption scheme based on discrete chaotic maps and AES. Discrete chaotic maps are used to achieve confusion and key generation to improve security.

In conclusion, the current retrieval of radar data based on deep learning and multichannel satellite data is not widely used, and the existing models do not make good use of the multiscale information of satellite data and do not take into account the interference brought by nonprecipitation clouds to the retrieval model, resulting in retrieval products that do not meet the expected results. In order to increase the retrieval accuracy and produce a dependable and RF retrieval result, it is important to develop an effective retrieval model.

III. Method

The framework of the privacy-preserving radar reflectivity retrieval method is shown in Fig. 1. First, the multichannel data collected by the satellite is encrypted by a key, and then, transmitted to the ground control station. The ground control station decrypts the encrypted satellite multichannel data using the same key. Finally, the decrypted data are input to the retrieval model to obtain the RF. In this section, we will introduce the privacy layer based on the AES encryption algorithm, then introduce a feature encode module employing MFM with an attention mechanism. Finally, we will introduce the decoder module that transforms the deep features of satellite data into the final retrieval results.

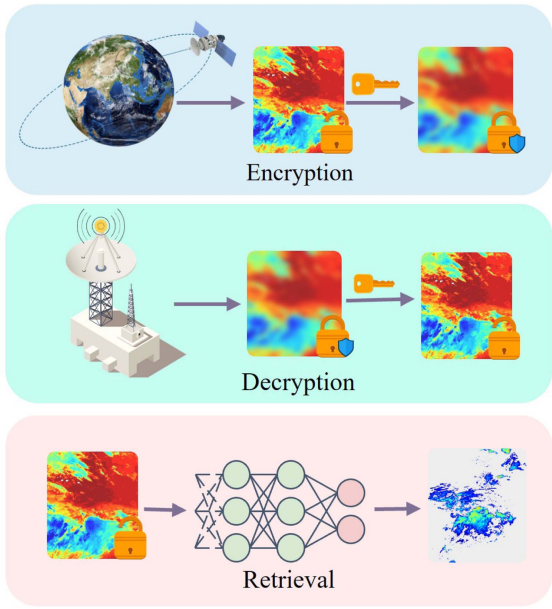

Fig. 1. Overview of the RF retrieval approach with privacy protection.

A. AES-Based Privacy Protection

Meteorological remote sensing satellites are used to acquire a vast array of information about the atmosphere, weather, and climate of the Earth. These data are frequently sensitive, and if insecure RF transmissions are employed, there is a risk of data leakage as well as data modification. AES is a commonly employed algorithm designed to prevent unauthorized data access. It is a symmetric encryption technique with multiple accessible key lengths. This study encrypts the transmission of remote sensing data with a 128-bit key in order to protect the real-time performance of remote sensing data. First, the AES algorithm groups the satellite-collected data D into $D = \{D_1, D_2, D_3, \ldots, D_N\}$ based on the 128-bit grouping (16 bytes). Then, the initial key K is enlarged into round keys $\{K_1, K_2, K_3, \ldots, K_N\}$, and each group is utilized individually. D_i will be encrypted using a different round key K_j for each of ten separate iterations. In each cycle of encryption, various fundamental operations, such as byte substitution, row shifting, column obfuscation, etc., will be performed. The final ciphertext C is composed of multiple encrypted groupings $C = \{C_1, C_2, C_3, \ldots, C_N\}$. The encrypted data can be transmitted safely through radio frequency.

The ground control station, upon receiving the ciphertext C, first sorts it into groups of $\{C_1, C_2, C_3, \ldots, C_N\}$, just as it did during encryption. Decryption of the ciphertext blocks occurs in multiple iterations using the same round key $\{K_1, K_2, K_3, \ldots, K_N\}$ used during encryption, and then, the plaintext blocks are stitched together to recover the original satellite data D.

B. Encode Module

Meteorological remote sensing data come from different sensors that use different frequency bands. This makes it hard to integrate and analyze them. Also, some factors can affect the

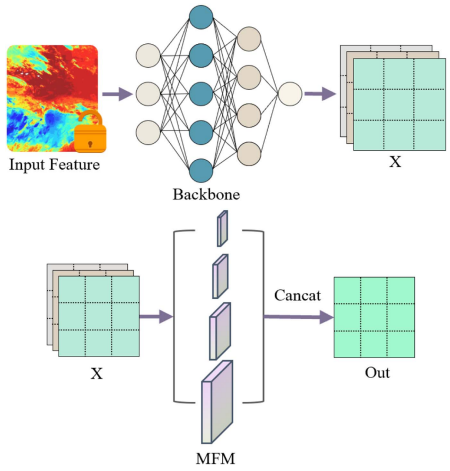

Fig. 2. Details of the encode module.

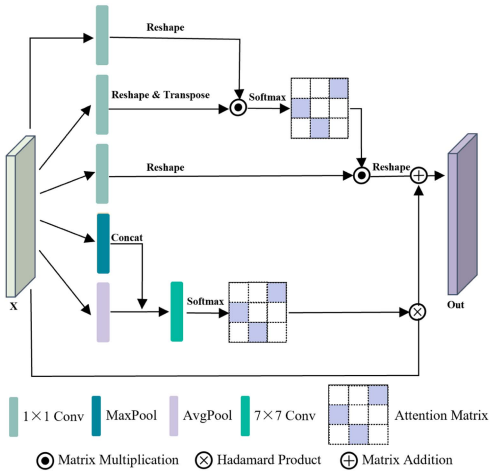

Fig. 4. Details of the spatial attention module.

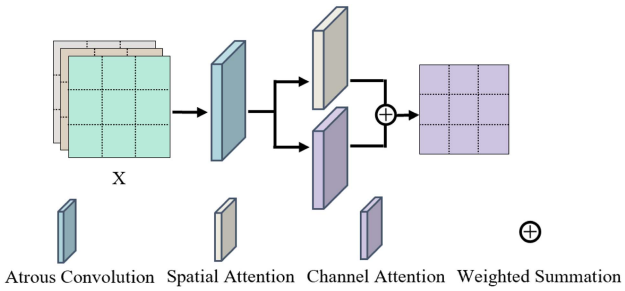

Fig. 3. Details of the MFM.

data quality, such as clouds that are not related to precipitation and solar radiation. Therefore, the remote sensing data received by the decoding module is processed by the encoder module to extract the deep semantic information contained within it.

The processing flow of the encode module is as shown in the Fig. 2. First, ResNet is used as the backbone network to extract deep semantic features. The last four downsampling layers of ResNet are replaced by four atrous convolutions, which enlarge the final feature map size to 1/8 of the input image, retaining more spatial details. Since the activity location and range of strong convection weather are different, after using the backbone network to extract deep information, a multiscale fusion module is used to further extract multiscale information of remote sensing data. In the multiscale feature fusion module, there are multiple scale information extraction modules, which obtain different scale information features through atrous convolutions with different sampling rates. Then, in order to better aggregate long-range context information, the current scale information feature is sent to the spatial attention module and channel attention module for parallel computation. Then, the calculation results of the two modules are weighted and summed to obtain the output result of the current scale. Finally, all scale outputs are concatenated to obtain the output of the encode module.

As shown in Fig. 3, the features $X \in \mathbb{R}^{C\times H\times W}$ obtained by the backbone network are further feature extracted by atrous convolution with different rates to obtain semantic information of different scales, where C represents the number of feature channels, H represents the height of the feature, and W represents the width of the feature. By using a spatial attention module after the scale information, the model can better aggregate the spatial context information by calculating the dependence relationship between the grid points in the space, emphasizing the areas with higher similarity in the grid points, and thus, emphasizing the grid points information that appears to have strong convective weather. At the same time, because the satellite data itself contain channels with large differences and the interference of nonprecipitation clouds in some channels is very strong, making it difficult for the model to effectively extract key information, in order for the model to more effectively use the more important channel information in the input features, use a channel attention module after the scale information to make the model able to pay attention to more critical channel information when there is interference information from nonprecipitation clouds in some channel data. It is worth noting that after obtaining the scale information through atrous convolution, the spatial attention module and channel attention module are calculated in parallel. The results obtained by both are weighted and summed to obtain the output result of the current scale.

Fig. 4 depicts the organization of the spatial attention module. The input feature $X \in \mathbb{R}^{C\times H\times W}$ is convolved with three 1×1 matrices to get three matrices $Q \in \mathbb{R}^{C\times H\times W}$, $K \in \mathbb{R}^{C\times H\times W}$, and $V \in \mathbb{R}^{C\times H\times W}$. The Q, K, and V matrix is then reshaped into $\mathbb{R}^{C\times N}$, where $N = H \times W$. The first part of the attention weight matrix is calculated as follows:

$$A_{s1} = \text{softmax}\left(K^T Q\right). \tag{1}$$

The second part performs the average pooling and maximum pooling of the input features X based on the spatial dimension, merges the two obtained feature information along the spatial dimension, performs a 7×7 convolution operation on the merged information, and obtains the attention weight matrix of this part by the Sigmoid activation function, which is calculated

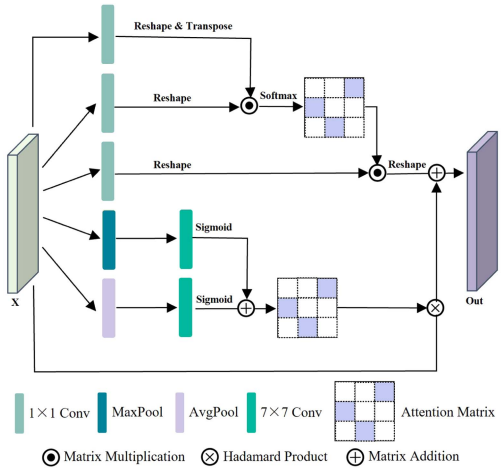

Fig. 5. Channel attention module.

as follows:

$$A_{s2} = \sigma\left(f^{7\times7}\left(\text{Concat}\left(\text{AvgPool}(X), \text{MaxPool}(X)\right)\right)\right) \quad (2)$$

where $f^{7\times7}$ is the 7×7 convolution.

The final output of the module is created by weighting and summing the outputs of the two sections of the computation, which is computed as follows:

$$\text{Out} = \text{Reshape}\left(\delta \times V \cdot A_{s1}\right) + \varphi \times A_{s2} \otimes X \quad (3)$$

where δ and φ are initially set to 0.01 as hyperparameters, which are then modified during training.

Fig. 5 depicts the construction of the channel attention module. The input feature $X \in \mathbb{R}^{C\times H\times W}$ is convolved with three 1×1 matrices to produce three matrices $Q \in \mathbb{R}^{C\times H\times W}$, $K \in \mathbb{R}^{C\times H\times W}$, and $V \in \mathbb{R}^{C\times H\times W}$. The Q, K, and V matrix is then reshaped into $\mathbb{R}^{C\times N}$, where $N = H \times W$, and the first portion of the attention weight matrix is computed as follows:

$$A_{c1} = \text{softmax}\left(QK^T\right). \quad (4)$$

The second part performs the average pooling and maximum pooling of the input features X based on the channel dimension, and the two information features obtained are passed through the Sigmoid activation function, respectively, their average values are then calculated to obtain the attention weight matrix of this part, which is calculated as follows:

$$A_{c2} = \frac{\sigma\left(f^{1\times1}\left(\text{AvgPool}(X)\right)\right) + \sigma\left(f^{1\times1}\left(\text{MaxPool}(X)\right)\right)}{2} \quad (5)$$

where $f^{1\times1}$ is the convolution of 1×1, and σ is the Sigmoid activation function.

The output of the module is the final weighted total of the two sections of the computation results, which is computed as follows:

$$\text{Out} = \text{Reshape}(\alpha \times A_{c1} \cdot V) + \beta \times A_{c2} \otimes X \quad (6)$$

where Reshape transforms the matrix into the form $\mathbb{R}^{C\times H\times W}$, $\cdot$ is the matrix multiplication, and $\otimes$ is the Hadamard product.

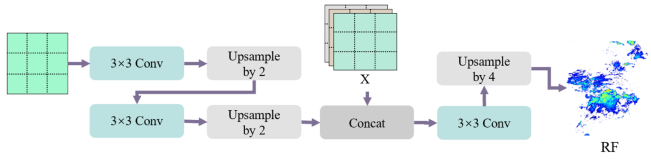

Fig. 6. Details of the decode module.

TABLE I
EXPERIMENTAL ENVIRONMENT

Experimental environment	Specific information
Operating system	Centos7
CPU	Intel(R) Core(TM) i9-10850k CPU at 3.60GH
GPU	NVIDIA TITAN V
Development language	Python3.8
Development platform	Pytorch1.11

The hyperparameters α and β are initially set to 0.01 and are modified throughout training.

C. Decode Module

Given that the final retrieval result is obtained by simply upsampling the encoder features, this retrieval retrieval may lose a significant amount of spatial information. To produce an accurate retrieval result, the encoder-obtained high-level semantic feature resolution must be gradually recovered by the decoder.

The details of the decode module are shown in Fig. 6. After the high-level semantic features obtained from the encoder have been refined using 3×3 convolution, the features are then upsampled twice using bilinear interpolation, and the 3×3 convolution operation is repeated once before being upsampled twice in order to make the feature size four times the initial value. After undergoing an upsampling process, the low-level semantic features that were initially received from the backbone network are then blended with the high-level semantic features that have the same resolution size. After that, the combined features are put through a process known as a 3×3 convolution, followed by a fourfold bilinear interpolation, so that the final retrieval results is obtained.

IV. EXPERIMENTS

To evaluate the effectiveness of the proposed retrieval model, we will conduct comprehensive experiments on the satellite-radar dataset from 2019 to 2022 in East China, including metric evaluation and specific retrieval case comparison. In the following subsections, we first introduce the experimental platform and dataset, then perform a series of ablation experiments, and finally, compare with other retrieval models.

A. Experimental Configuration

Table I shows the environment of the experiment.The geostationary meteorological satellite data utilized in this model are the Himawari-8 satellite's full-disk scan grid data. The satellite grid data consist of 16 channels in the visible, near-infrared, and infrared bands, and as each channel of the Himawari-8 AHI

sensor has a distinctive observation band, the resulting data include distinct identifying information. Since including all satellite data channels into the retrieval model would significantly raise the training cost and hardware burden of the network, training and retrieval times will be extended. In addition, the limited observation duration of visible channels and the inclusion of too duplicated information in particular channels can have a significant impact on the model's precision. Therefore, in this research, the Himawari-8 grid point data for 16 channels are reviewed. In this article, the bright temperature difference (BTD) between 11 and 6.7 μm channels is used to identify deep convective clouds capable of producing heavy rainfall by Kurino [25]; the BTD between 6.9- and 10.7 μm channels is used to identify upwelling cloud tops by Ba et al. [15]; Mecikalski et al. [26] employed the BTD between several infrared channels of the Meteosat-9 satellite as a measure of cloud thickness. Therefore, we eliminate the visible channels and data channels with low correlation with radar reflectivity, and select the following four channels of data: 7, 9, 13, and 16. Additionally, we introduce the BTD data of channels 14-9 and 13-9 with a spatial resolution of 0.04° and a temporal resolution of 10 min. The time range is from 2020 to 2022. Channel 7 is a short-wave infrared, channel data with particle radius, with a central wavelength of 3.90 μm, primarily for lower cloud observations; channel 9 is a water vapor band, with a central wavelength of 6.95 μm, primarily for midlevel water vapor level observations; channels 13 and 14 are infrared windows, with a central wavelength of 10.35 and 11.2 μm, respectively, primarily for cloud images and cloud top situation observations; and channel 16 is a CO_2 window with a center wavelength of 13.30 μm and is primarily used for cloud height measurements. Considering that cirrus clouds, as high-level non-precipitating clouds, have very low cloud top temperatures but do not bring rainfall, which can cause great disturbances to the retrieval model, it is necessary to minimize the disturbances of cirrus clouds as much as possible. On the basis of Kurino [25], who used the BTD between channels 11 and 12 of the Geostationary Meteorological Satellite (GMS-5) to reduce the interference of upper level nonprecipitation clouds, the model presented in this article is trained with the BTD between channels 13 and 15 of similar wavelength.

We use radar network data from eastern China for this study, with longitude range of 108°N–125°N and latitude range of 20°N–40°N, due to the limited detection range of radars, the scarcity of radars in southwest China, and the variable completeness of radar data across different regions. The spatial resolution is 0.04°, so the input of the model is matched and cropped to a size of 425 × 500. In addition, the temporal resolution of the radar data is 6 min. However, the temporal resolution of the radar network data and the satellite grid data are not identical, and matching only the data with the same temporal resolution will lead to insufficient data samples for training the model. Since the atmospheric motion does not change much in a short time, we match the satellite data with the closest time when there is no satellite data with the same time as the radar data. For example, we match radar data at 8:10 with satellite data at 8:12.

B. Evaluation Indicators

Following [11], we evaluate the retrieval results using five evaluation indicators that are commonly used in meteorology: probability of detection (POD), critical success index (CSI), false alarm ratio (FAR), accuracy (ACC), and Heidke skill score (HSS). These indicators measure the accuracy, stability and reliability of the retrieval model. We binarize the radar reflectivity values by a threshold τ: 1 for values above τ and 0 for values below τ. We then compare the binarized values with the ground truth and count the true positives (TP), false positives (FP), true negatives (TN), and false negatives (FN). The calculation of the evaluation indexes is as follows:

$$\mathrm{POD} = \frac{\mathrm{TP}}{(\mathrm{TP}+\mathrm{FN})} \tag{7}$$

$$\mathrm{FAR} = \frac{\mathrm{FP}}{(\mathrm{FP}+\mathrm{TP})} \tag{8}$$

$$\mathrm{CSI} = \frac{\mathrm{TP}}{(\mathrm{TP}+\mathrm{FP}+\mathrm{FN})} \tag{9}$$

$$\mathrm{ACC} = \frac{(\mathrm{TP}+\mathrm{TN})}{(\mathrm{TP}+\mathrm{FN}+\mathrm{FP}+\mathrm{TN})} \tag{10}$$

$$\mathrm{HSS} = \frac{2\times(\mathrm{TP}\times\mathrm{TN}-\mathrm{FN}\times\mathrm{FP})}{(\mathrm{FN}+\mathrm{FP})\times(\mathrm{TP}+\mathrm{TN}+2)}. \tag{11}$$

C. Loss Function

Due to the fact that the significance of radar reflectivity changes for different values, for instance, an RF larger than 35 dBZ indicates the presence of severe convective weather, which impacts all human activities. The retrieval model must pay special attention to regions with higher radar reflectivity; thus, the retrieval model is trained using a weighted squared difference loss function in all experiments to improve the model's capacity to retrieve bigger RF, as follows:

$$\mathrm{loss} = \frac{1}{n}\sum_{i=1}^{n} w(y)\otimes(y-y^p)^2 \tag{12}$$

where y represents the observed radar reflectivity of a grid, y^p represents the projected radar reflectivity of the retrieval model for the same grid, and $w(y)$ represents the weight value derived from the observed radar reflectivity, and the calculation rule is shown as follows:

$$w(y) = \begin{cases} 1 & \mathrm{dBZ}(\mathrm{REF}=0) < y < \mathrm{dBZ}(\mathrm{REF}=5) \\ 10 & \mathrm{dBZ}(\mathrm{REF}=5) <= y < \mathrm{dBZ}(\mathrm{REF}=20) \\ 15 & \mathrm{dBZ}(\mathrm{REF}=20) <= y < \mathrm{dBZ}(\mathrm{REF}=35) \\ 70 & \mathrm{dBZ}(\mathrm{REF}=35) <= y < \mathrm{dBZ}(\mathrm{REF}=50) \\ 500 & \mathrm{dBZ}(\mathrm{REF}=50) <= y < \mathrm{dBZ}(\mathrm{REF}=80) \end{cases} \tag{13}$$

where $w(y)=1$ represents clear weather, $w(y)=10$ represents light rain, $w(y)=15$ represents light to moderate rain, $w(y)=70$ represents heavy to torrential rain, and $w(y)=500$ represents very heavy rainfall hail and other powerful convective weather.

TABLE II
COMPARISON OF THE RETRIEVAL RESULTS OF MFM WITH VARIOUS RC SETTINGS WHEN τ IS SET TO 35

Backbone	RC	POD	FAR	CSI	HSS	ACC
ResNet50	None	0.32	0.63	0.15	0.21	0.96
ResNet50	{1}	0.36	0.58	0.21	0.26	0.96
ResNet50	{1,3}	0.42	0.52	0.29	0.37	0.97
ResNet50	{1,3,6}	0.45	0.53	0.32	0.45	0.98
ResNet50	{1,3,6,12}	**0.56**	0.45	**0.35**	**0.52**	**0.99**
ResNet50	{1,3,6,12,16}	0.54	**0.44**	0.34	0.51	**0.99**
ResNet101	{1,3,6,12}	**0.63**	**0.36**	**0.49**	**0.55**	**0.99**

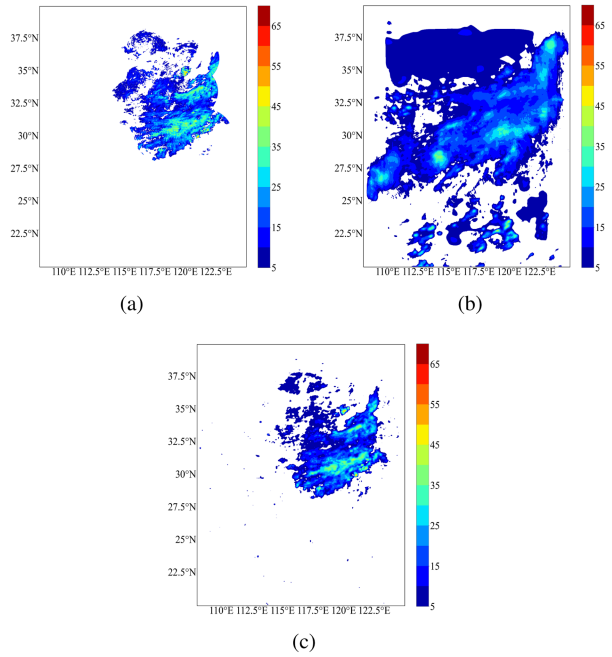

Fig. 7. Comparison of the retrieval results between the baseline FCN model and MARRN. (a) Reference observation. (b) Baseline FCN. (c) MARRN.

D. Ablation Study

In this article, experiments with different settings were conducted to evaluate the effectiveness of the MFM proposed in the encoder module. Our baseline was the ResNet50-based fully convolutional network (FCN) expansion network [27]. The retrieval results of the MFM under various sample rate combination (RC) settings with a fixed decoder module and $\tau =$ 35 are presented in Table II, where the best results are marked in bold. Table II reveals, first, all retrieval models with MFM greatly outperformed the baseline FCN in terms of retrieval performance. Second, the optimal sample RC was {1,3,6,12}, which increased the performance of the FCN baseline by 79.81% on average. The MFM accurately captures the features of intense convective weather and enhances the model's retrieval accuracy. In the subsequent experiments, we adopt MFM with sampling RCs of {1,3,6,12}, and use ResNet101 as the backbone of the model. To distinguish our retrieval model from other models, we name it multiscale attention RF retrieval model (MARRN). Fig. 7 illustrates a comparison between the real retrieval scenarios of the baseline FCN and the MARRN.

TABLE III
COMPARISON OF DIFFERENT DECODER STRATEGIES WHEN τ IS SET TO 35

Decoder	POD	FAR	CSI	HSS	ACC
Direct resolution recovery	0.55	0.45	0.31	0.52	**0.99**
Ours	**0.63**	**0.36**	**0.49**	**0.55**	**0.99**

In a similar manner, we contrasts the resolution recovery technique that maintains the encoder with the proposed decoder module, with τ also set to 35, as shown in Table III. The decoder module described in this study has increased the retrieval model's accuracy by 6.5% compared to the direct resolution recovery technique, as shown in Table III. It may be concluded that the decoder module introduced in this work increases the retrieval model's accuracy.

E. Compare With Other Models

Using the same dataset, we will compare the retrieval performance of our model to that of other retrieval models. As comparison models, we will use the U-Net algorithm [28] and the DeepLabV3 method [29]. The U-Net employs an encoder–decoder architecture in which the encoder collects deep semantic information via repetitive downsampling and the decoder restores resolution by repeated upsampling. To retain the set resolution, the DeepLabV3 model converts the last four blocks of ResNet to hollow convolution, and then, employs parallel hollow convolution layers with varying sampling rates to collect multiscale semantic information, effectively combining multiscale satellite data features.

As shown in Fig. 8, when the threshold is set to 5 and 20, the model in this article only improves by 1.4 and 4.4 percentage points in POD score compared with DeepLabV3, but when the threshold is set to a larger value of 35, the model in this article improves by 17 percentage points, and other evaluation indicators also have a consistent phenomenon. This shows that the weighted loss function and the attention mechanism in the model play a role, making the model more effective in focusing on areas with strong radar reflectivity.

Figs. 9 and 10 display the retrieval outcomes of distinct methods for the same time points on June 11, 2021 at 8:50 A.M. and June 25, 2021 at 19:00 P.M., respectively. According to the data, the U-Net algorithm has the worst retrieval impact, with several false alarms. This is due to the fact that the U-Net structure can only recover low-resolution representations by recurrent upsampling, which makes it challenging to compensate for spatial resolution losses. Even though the U-Net introduces cross-layer connections to combine shallow-layer features with high-level abstract features, it is challenging to fully understand the characteristics of clouds that bring intense convective weather in the face of satellite data with interference from nonprecipitation clouds. In the precipitation area, the DeepLabV3 algorithm is largely consistent with the reference observation, although there are still some false alarms and missing reports in certain regions. Although the DeepLabV3 approach adds a hole-space pyramid structure to extract features at different resolutions, it does not adequately incorporate global context, making it challenging for

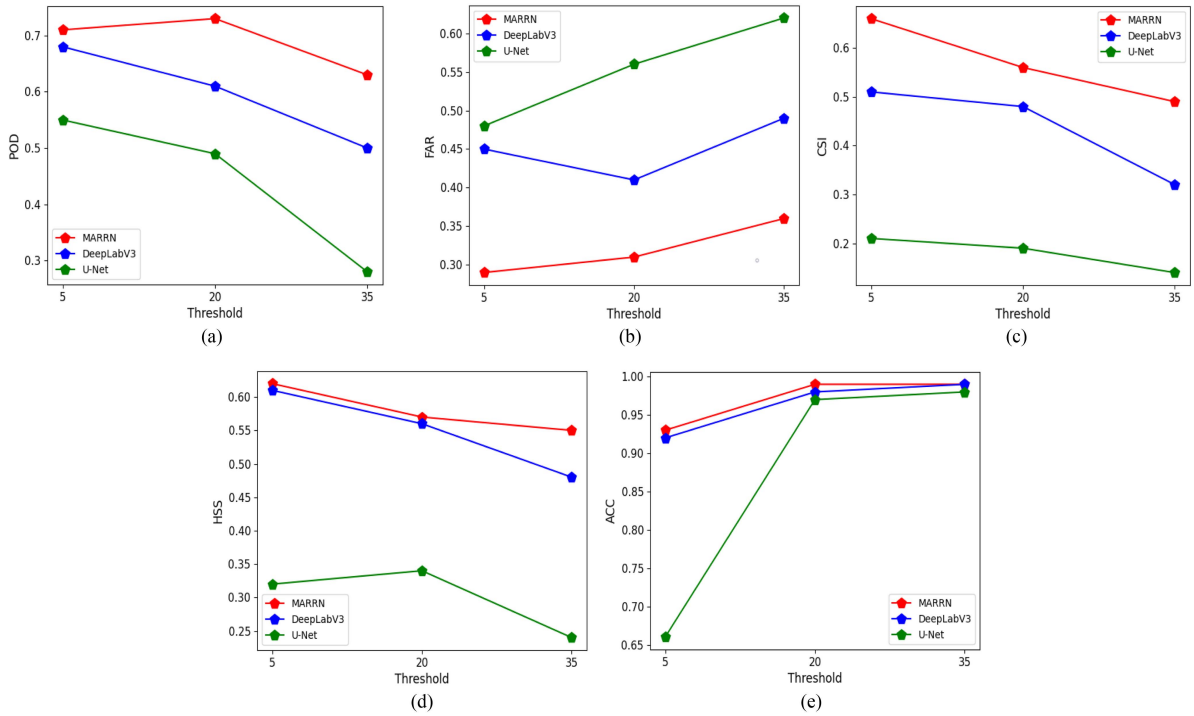

Fig. 8. Comparison of the scores of different models for each index. (a) POD scores of each model under different thresholds. (b) FAR scores of each model under different thresholds. (c) CSI scores of each model under different thresholds. (d) HSS scores of each model under different thresholds. (e) ACC scores of each model under different thresholds.

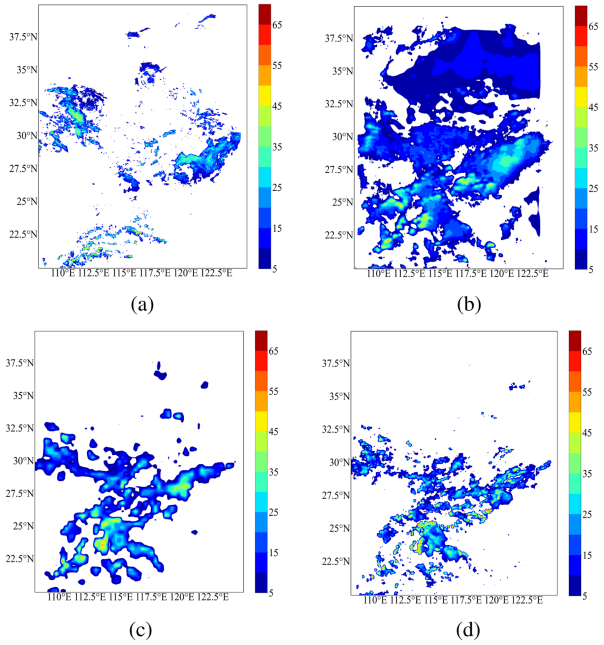

Fig. 9. June 11th, 2021, 8:50 A.M. study case. (a) Reference observation. (b) U-Net. (c) DeepLabV3. (d) MARRN.

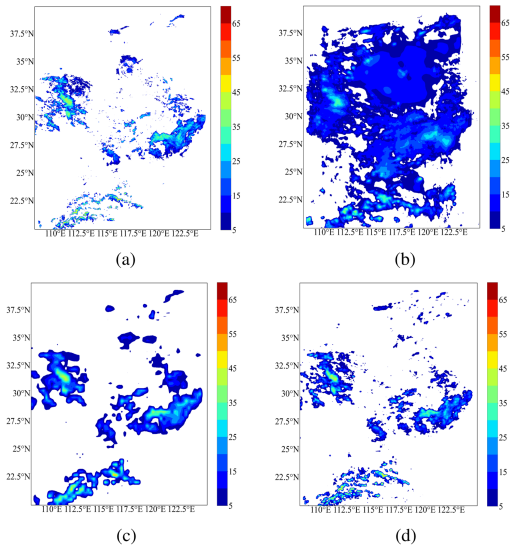

Fig. 10. June 25th, 2021 at 19:00 P.M. study case. (a) Reference observation. (b) U-Net. (c) DeepLabV3. (d) MARRN.

the model to avoid interference from nonprecipitation high-level clouds. Compared to previous models, the results of the MARRN are more precise and accurate in spatial distribution, but there are still missed reports in areas with small reflectivities, which may be due to the model's inability to accurately distinguish between nonprecipitating clouds and precipitating clouds.

V. Conclusion

In this study, we present a novel model for retrieval radar reflectivity from multichannel satellite data, based on the assumption that multichannel data of meteorological satellites can capture the information of RF. Our model leverages multiscale feature fusion to effectively extract the multiscale features of the satellite data, and incorporates an attention mechanism in the fusion module, which allows the model to focus on the features that are directly relevant to the radar reflectivity and filter out the

noise from nonprecipitation clouds, by exploiting the spatial and channel context of the satellite data. To address the privacy issue of satellite data transmission, we apply the AES to the satellite to protect the collected data from unauthorized access. We demonstrate that our model outperforms the baseline methods in all evaluation metrics. We also discuss the future work of further eliminating the effects of cloud layer, atmosphere, surface, and other factors on satellite data.

REFERENCES

[1] A. Choryński, I. Pińskwar, D. Graczyk, and M. Krzyżaniak, "The emergence of different local resilience arrangements regarding extreme weather events in small municipalities—A case study from the Wielkopolska region, Poland," *Sustainability*, vol. 14, no. 4, 2022, Art. no. 2052.

[2] L. Yi et al., "Parameterized tropical cyclone precipitation model for catastrophe risk assessment in China," *J. Appl. Meteorol. Climatol.*, vol. 61, no. 9, pp. 1291–1303, 2022. [Online]. Available: https://journals.ametsoc.org/view/journals/apme/61/9/JAMC-D-21-0157.1.xml

[3] G. Hu et al., "Progress, challenges, and future steps in data assimilation for convection-permitting numerical weather prediction: Report on the virtual meeting held on 10 and 12," 2021 *Atmospheric Sci. Lett.*, vol. 24, no. 1, 2023, Art. no. e1130.

[4] K. Zhao et al., "Recent progress in dual-polarization radar research and applications in China," *Adv. Atmospheric Sci.*, vol. 36, no. 9, pp. 961–974, 2019.

[5] M. S. Binetti, C. Campanale, C. Massarelli, and V. F. Uricchio, "The use of weather radar data: Possibilities, challenges and advanced applications," *Earth*, vol. 3, no. 1, pp. 157–171, 2022.

[6] S. Ravuri et al., "Skilful precipitation nowcasting using deep generative models of radar," *Nature*, vol. 597, no. 7878, pp. 672–677, 2021.

[7] C. Min et al., "Coverage of China new generation weather radar network," *Adv. Meteorol.*, vol. 2019, pp. 1–10, Jun. 2019.

[8] J. R. Eyre, S. J. English, and M. Forsythe, "Assimilation of satellite data in numerical weather prediction. Part I: The early years," *Quart. J. Roy. Meteorological Soc.*, vol. 146, no. 726, pp. 49–68, 2020.

[9] M. W. Maier et al., "Architecting the future of weather satellites," *Bull. Amer. Meteorological Soc.*, vol. 102, no. 3, pp. E589–E610, 2021.

[10] H. Jiang, N. Lu, J. Qin, W. Tang, and L. Yao, "A deep learning algorithm to estimate hourly global solar radiation from geostationary satellite data," *Renewable Sustain. Energy Rev.*, vol. 114, 2019, Art. no. 109327.

[11] M. Duan et al., "Reconstruction of the radar reflectivity of convective storms based on deep learning and Himawari-8 observations," *Remote Sens.*, vol. 13, no. 16, 2021, Art. no. 3330.

[12] L. Yang et al., "Radar composite reflectivity reconstruction based on FY-4A using deep learning," *Sensors*, vol. 23, no. 1, 2023. [Online]. Available: https://www.mdpi.com/1424-8220/23/1/81

[13] M. W. Kimani, J. C. B. Hoedjes, and Z. Su, "Bayesian bias correction of satellite rainfall estimates for climate studies," *Remote Sens.*, vol. 10, no. 7, 2018. [Online]. Available: https://www.mdpi.com/2072-4292/10/7/1074

[14] J. Long, E. Shelhamer, and T. Darrell, "Fully convolutional networks for semantic segmentation," in *Proc. Conf. Comput. Vis. Pattern Recognit.*, 2015, pp. 3431–3440.

[15] M. B. Ba and A. Gruber, "Goes multispectral rainfall algorithm (GMSRA)," *J. Appl. Meteorol.*, vol. 40, no. 8, pp. 1500–1514, 2001. [Online]. Available: https://journals.ametsoc.org/view/journals/apme/40/8/1520-0450_2001_040_1500_gmrag_2.0.co_2.xml

[16] E. E. Ebert and M. J. Manton, "Performance of satellite rainfall estimation algorithms during TOGA COARE," *J. Atmospheric Sci.*, vol. 55, no. 9, pp. 1537–1557, 1998.

[17] F. Torricella, E. Cattani, and V. Levizzani, "Rain area delineation by means of multispectral cloud characterization from satellite," *Adv. Geosci.*, vol. 17, pp. 43–47, 2008.

[18] B. Thies, T. Nauß, and J. Bendix, "Precipitation process and rainfall intensity differentiation using meteosat second generation spinning enhanced visible and infrared imager data," *J. Geophys. Res., Atmospheres*, vol. 113, no. D23, pp. 1–19, 2008.

[19] H. Feidas and A. Giannakos, "Classifying convective and stratiform rain using multispectral infrared meteosat second generation satellite data," *Theor. Appl. Climatol.*, vol. 108, no. 3, pp. 613–630, 2012.

[20] M. Lazri, Z. Ameur, S. Ameur, Y. Mohia, J. M. Brucker, and J. Testud, "Rainfall estimation over a mediterranean region using a method based on various spectral parameters of SEVIRI-MSG," *Adv. Space Res.*, vol. 52, no. 8, pp. 1450–1466, 2013.

[21] M. S. Veillette, E. P. Hassey, C. J. Mattioli, H. Iskenderian, and P. M. Lamey, "Creating synthetic radar imagery using convolutional neural networks," *J. Atmospheric Ocean. Technol.*, vol. 35, no. 12, pp. 2323–2338, 2018.

[22] F. Sun, B. Li, M. Min, and D. Qin, "Deep learning-based radar composite reflectivity factor estimations from Fengyun-4A geostationary satellite observations," *Remote Sens.*, vol. 13, no. 11, 2021, Art. no. 2229.

[23] S. Jeon, J. Kwak, and J. P. Choi, "Cross-layer encryption of CFB-AES-TURBO for advanced satellite data transmission security," *IEEE Trans. Aerosp. Electron. Syst.*, vol. 58, no. 3, pp. 2192–2205, Jun. 2021.

[24] E. Bensikaddour and Y. Bentoutou, "Satellite image encryption based on AES and discretised chaotic maps," *Automat. Control Comput. Sci.*, vol. 54, pp. 446–455, 2020.

[25] T. Kurino, "A satellite infrared technique for estimating "deep/shallow" precipitation," *Adv. Space Res.*, vol. 19, no. 3, pp. 511–514, 1997.

[26] J. R. Mecikalski, W. M. MacKenzie, M. Koenig, and S. Muller, "Cloud-top properties of growing cumulus prior to convective initiation as measured by meteosat second generation. Part I: Infrared fields," *J. Appl. Meteorol. Climatol.*, vol. 49, no. 3, pp. 521–534, 2010.

[27] W. Luo, Y. Li, R. Urtasun, and R. Zemel, "Understanding the effective receptive field in deep convolutional neural networks," in *Proc. 30th Int. Conf. Neural Inf. Process. Syst.*, 2016, pp. 4905–4913. [Online]. Available: https://proceedings.neurips.cc/paper_files/paper/2016/file/c8067ad1937f728f51288b3eb986afaa-Paper.pdf

[28] O. Ronneberger, P. Fischer, and T. Brox, "U-Net: Convolutional networks for biomedical image segmentation," in *Proc. Int. Conf. Med. Image Comput. Comput.-Assisted Intervention*, 2015, pp. 234–241.

[29] L.-C. Chen, G. Papandreou, F. Schroff, and H. Adam, "Rethinking atrous convolution for semantic image segmentation," 2017, *arXiv:1706.05587*.

Huichao Lin is currently working toward the master degree in computer science with the School of Software, Nanjing University of Information Science and Technology, Nanjing, China.

His research interests include remote sensing, machine learning, and Big Data.

Xiaolong Xu (Senior Member, IEEE) received the Ph.D. degree in computer science and technology from Nanjing University, Nanjing, China, in 2016.

He was a Research Scholar with Michigan State University, USA, from 2017 to 2018. He is currently a Full Professor with the School of Software, Nanjing University of Information Science and Technology, Nanjing. He has authored and co-authored more than 100 peer-review articles in international journals and conferences, including IEEE TRANSACTIONS ON PARALLEL AND DISTRIBUTED SYSTEMS, IEEE TRANSACTIONS ON INTELLIGENT TRANSPORTATION SYSTEMS, IEEE TRANSACTIONS ON INDUSTRIAL INFORMATICS, *ACM Transactions on Sensor Networks*, *ACM Transactions on Multimedia Computing, Communications, and Applications*, *ACM Transactions on Intelligent Systems and Technology*, IEEE International Conference on Web Services, International Conference on Service-Oriented Computing, etc.

Dr. Xu was selected as the Highly Cited Researcher of Clarivate 2021 and 2022. He was the recipient of the top citation award from *Computational Intelligence Journal*, the Best Paper Awards from 2016 IEEE International Conference on Advanced Cloud and Big Data, 2020 IEEE International Conference on Cyber, Physical and Social Computing, 2020 International Conference on Security and Privacy in Digital Economy, 2021 IEEE Cyber Science and Technology Congress, 2022 IEEE International Conference on Advanced Technologies for Communications, 2022 IEEE International Conferences on Internet of Things, 2021 International Conference on Computer Engineering and Networks, and 2021 EAI International Conference on Cloud Computing (EAI Cloudcomp) and the Best Student Paper Award from EAI Cloudcomp 2019, and the Best Session Paper from 2020 IEEE International Conference on Data Science and Advanced Analytics. He was also the recipient of the Outstanding Leadership Award from 2022 IEEE International Conference on Ubiquitous Intelligence and Computing.

Muhammad Bilal (Senior Member, IEEE) received the Ph.D. degree in information and communication network engineering from the School of Electronics and Telecommunications Research Institute (ETRI), Korea University of Science and Technology, Daejeon, South Korea, in 2017.

From 2017 to 2018, he was with Korea University, where he was a Postdoctoral Research Fellow with the Smart Quantum Communication Center. In 2018, he joined the Hankuk University of Foreign Studies, South Korea, where he is currently working as an Associate Professor with the Division of Computer and Electronic Systems Engineering. He is the author/co-author of more than 100 articles published in renowned journals, one book editorship, three issued US patents, and six Korean patents. His research interests include network optimization, cyber security, Internet of Things, vehicular networks, information-centric networking, digital twin, artificial intelligence, and Cloud/Fog computing.

Dr. Bilal is an editorial board member of IEEE TRANSACTIONS ON INTELLIGENT TRANSPORTATION SYSTEMS, IEEE FUTURE DIRECTIONS IN TECHNOLOGY, POLICY, AND ETHICS NEWSLETTER, *Alexandria Engineering Journal* (Elsevier), *Physical Communication* (Elsevier), *Computer Systems Science and Engineering*, *Intelligent Automation and Soft Computing*, *Frontiers in Communications and Networks*, *Frontiers in the Internet of Things*, and a co-Editors-in-Chief of *International Journal of Smart Vehicles and Smart Transportation*.

Yong Cheng received the Ph.D. degree in computer science and technology from Wuhan University, Wuhan, China, in 2009.

He is currently a Full Professor with the School of Software, Nanjing University of Information Science and Technology, Nanjing, China. He has authored and co-authored some articles in international journals, including the IEEE INTERNET OF THINGS JOURNAL, etc. His research interests include Big data, Internet of Things, and deep learning.

Dongqing Liu received the MA.Sc. degree in atmospheric science from Nanjing University, Nanjing, China, in 2010.

He is currently working with Nanjing Meteorological Bureau as the Deputy Director of meteorological observatory. He is mainly involved in the research on application of artificial intelligence in weather forecast and retrieval of radar reflectivity.